Calculation of Consistent Flux and Advective Terms from Adjusted Vertical Profiles of Divergence

JOHN MOLINARI AND STEVEN SKUBIS

Department of Atmospheric Science, State University of New York at Albany, Albany, New York

(Manuscript received 20 August 1987, in final form 25 October 1987)

ABSTRACT

A simple framework is presented for adjusting the normal wind components in a polygon of data points which produces a vanishing vertical integral of horizontal divergence, allows correct calculation of flux and advective terms, and permits virtually any choice of vertical profile of divergence adjustment. The procedure was used to estimate precipitation as a residual from vertically integrated heat and moisture budgets for SESAME data, in order to evaluate the uncertainty introduced by commonly used approximations in diagnostic studies. Although the method cannot be applied on a grid in its current form, the results remain valid for gridded calculations.

Line integrals around the polygon were carried out analytically, allowing an exact calculation of eddy fluxes within the assumption of linearity along the edges. Finite difference approximations for nonlinear terms were shown to introduce significant errors, even under ordinary circumstances.

It is common practice to neglect the horizontal advecting velocity adjustment brought about by the adjusted divergence. Such an assumption produced negligible median errors in the integrated heat and moisture budgets. The median differences in calculated precipitation caused by differing choices of the divergence adjustment profile reached 1.34 and 0.35 cm day^{-1} in the heat and moisture budgets, respectively. Because the true divergence adjustment profile is unknown, these values represent median lower bounds on the errors in budget estimates of precipitation in middle latitude convection.

1. Introduction

It is well known that vertical integration of the mass conservation equation to obtain the p-system vertical velocity ω is confounded by errors in calculated horizontal divergence caused by measurement and analysis errors in the winds. In real-data diagnostic studies, these errors invariably produce a column-mean divergence (and by implication, a pressure tendency at column top or bottom) far in excess of that observed. To eliminate this problem, the vertical profile of divergence must be adjusted to produce zero (or small) integrated divergence. Although an infinite number of adjustments exist which satisfy this constraint, a constant or linearly increasing divergence error in the vertical is usually assumed (O'Brien 1970).

Once the divergence is adjusted, it becomes necessary to recalculate the horizontal wind vector to ensure consistency with the adjusted divergence, if both are used in subsequent computations. In studies using gridded data, the adjusted horizontal wind vector has been recovered by one of two methods: by calculating a rotational and divergent wind, replacing the original divergent wind with its adjusted value, and recombining (e.g., Krishnamurti et al. 1979); or by reconstructing the wind via variational calculus techniques (e.g., Stephens 1968) which constrain the integrated divergence to zero while minimizing changes in the wind (Ray et al. 1980).

For observational studies which use fixed polygons of data points, such as those in GATE, ATEX, and other special data collections, the above procedures cannot be directly applied, and it is almost universal practice to neglect the change in the horizontal advecting velocity brought about by adjustments of the horizontal divergence. Only McNab and Betts (1978) made the necessary adjustments, but they required an arbitrary assumption that divergence error was evenly divided between u and v components of the wind. The neglect of internally consistent wind adjustments by other researchers produces errors in advective terms and in budget equation residuals whose magnitude has not been investigated.

In either gridded or polygon calculations, the assumed form of the divergence adjustment introduces errors, because the true divergence error profile from rawinsondes or other measurement platforms is unknown and probably a complex function of the flow field. Smith (1971) subjectively correlated observed precipitation with vertical motion fields computed using two divergence adjustment methods, and concluded that a linear increase in divergence error with decreas-

Corresponding author address: Dr. John Molinari, Dept. of Atmospheric Science, State University of New York at Albany, Earth Science 219, Albany, NY 12222.

ing pressure gave more realistic vertical velocities than a constant profile of divergence error. Statistical arguments by Pedder (1981) suggest, however, that little is gained even by physically reasonable divergence adjustment profiles, compared with a simple constant adjustment. No study has quantitatively evaluated the uncertainty introduced by the form of the divergence adjustment.

The current work addresses the above problems for a polygon of observation points by proposing a framework for satisfying zero integrated divergence which directly adjusts the components of the wind normal to the polygon edges. This framework provides a means of calculating all terms in the budget equation consistent with the adjusted divergence while allowing virtually any choice of divergence adjustment profile. The proposed method is applied to the SESAME dataset in order to determine typical errors in heat and moisture budgets produced both by neglect of the divergence adjustment in the horizontal advecting velocity and by the form of the divergence adjustment.

2. Errors associated with divergence adjustments

Using specific humidity q as an example, a budget equation can be written

$$\frac{\partial \bar{q}}{\partial t} = -\overline{\nabla_p \cdot q\mathbf{v}} - \frac{\partial}{\partial p}\overline{q\omega} - (c - e) \tag{1}$$

where the overbar indicates an average over the polygon, and c and e are rates of condensation and evaporation. A common use for such an equation is to estimate mean precipitation over an area as a residual from the vertical integral, i.e.,

$$P \equiv \frac{1}{g}\int_{p_{top}}^{p_s} (c - e)dp$$

$$= \frac{1}{g}\int_{p_{top}}^{p_s} -\left[\frac{\partial \bar{q}}{\partial t} + \overline{\mathbf{v}\cdot\nabla_p q} + \overline{q\nabla_p\cdot\mathbf{v}}\right]dp + E_0 \tag{2}$$

where surface evaporation rate E_0 arises from the vertically integrated vertical eddy flux, $\bar{\omega} = 0$ has been assumed at p_s (surface pressure) and p_{top} (pressure at some level near the tropopause), the horizontal flux convergence term has been expanded into advective and divergent components, and liquid water storage has been neglected. In order for (2) to be strictly valid, the divergence field must be adjusted to satisfy the $\bar{\omega}$ boundary conditions. Because $\bar{\omega}$ is obtained from

$$\frac{\partial \bar{\omega}}{\partial p} = -\overline{\nabla_p \cdot \mathbf{v}} \tag{3}$$

the divergence must satisfy

$$\int_{p_{top}}^{p_s} \overline{\nabla_p \cdot \mathbf{v}}dp = 0 \tag{4}$$

and $\mathbf{v}$ must be recalculated to be consistent with the adjusted divergence.

As noted earlier, when the adjusted divergence is substituted into the divergence term in (2), the adjustment of the horizontal advecting velocity is almost always neglected (e.g., Nitta 1977; Frank 1979). Denoting the unadjusted wind as $\mathbf{v}^*$ and the adjusted wind as $\mathbf{v}$, the resultant precipitation estimate becomes

$$P^* = \frac{1}{g}\int_{p_{top}}^{p_s} -\left[\frac{\partial \bar{q}}{\partial t} + \overline{\mathbf{v}^*\cdot\nabla_p q} + \overline{q\nabla_p\cdot\mathbf{v}}\right]dp + E_0 \tag{5}$$

producing an error of magnitude

$$P^q_{err} = |P^* - P| = \frac{1}{g}\left|\int_{p_{top}}^{p_s} -\overline{(\mathbf{v}^* - \mathbf{v})\cdot\nabla_p q}dp\right| \tag{6}$$

where the superscript refers to a moisture budget calculation. An analogous error in precipitation rate arises in a potential temperature budget:

$$P^\theta_{err} = \frac{c_p}{Lg}\left|\int_{p_{top}}^{p_s} -\frac{T}{\theta}\left[\overline{(\mathbf{v}^* - \mathbf{v})\cdot\nabla_p\theta}\right]dp\right|. \tag{7}$$

Even when consistent adjustments are made in all occurrences of $\mathbf{v}$, an error arises from the choice of a divergence adjustment. This error will be estimated in the current study by comparing precipitation calculated from two different divergence adjustment profiles. It can be seen from (2) that the resultant precipitation difference takes the form

$$P^q_{diff} = \frac{1}{g}\left|\int_{p_{top}}^{p_s} \left[\overline{\nabla_p\cdot q(\mathbf{v}^{(\epsilon)} - \mathbf{v}^{(C)})}\right]dp\right| \tag{8}$$

where the ϵ and C superscripts refer to two divergence adjustment methods described in section 3. The small difference in E_0 due to the form of divergence adjustment has been neglected in (8). The analogous quantity in the potential temperature budget can be written as

$$P^\theta_{diff} = \frac{c_p}{Lg}\left|\int_{p_{top}}^{p_s} \frac{T}{\theta}\left[\overline{\nabla_p\cdot\theta(\mathbf{v}^{(\epsilon)} - \mathbf{v}^{(C)})}\right]dp\right|. \tag{9}$$

The errors arising from neglect of the advecting velocity adjustments in (6)–(7) will be evaluated using both forms of adjusted wind ($\mathbf{v}^{(\epsilon)}$ and $\mathbf{v}^{(C)}$), while (8)–(9) will provide a measure of the influence of the divergence adjustment profile alone. The term "precipitation error" in this paper will not represent the difference between calculated and observed precipitation, but rather the differences in precipitation rate which arise solely from the assumptions made in calculation procedures. Such methodological errors must be small for the calculated precipitation to be meaningful.

3. Description of the method

a. Adjustment procedures

Given a triangle or other polygon of data points, the goal is to determine a consistent budget for which divergence adjustments have been incorporated into all

appropriate terms. The area-averaged divergence can be written

$$\bar{D} = \frac{\int_A \nabla_p \cdot \mathbf{v}\, dA}{\int_A dA} = \frac{\oint v_n ds}{A} \tag{10}$$

where v_n are the components normal to the face of the polygon and s is distance around the edge. From (4) and (10), the normal components must satisfy

$$\int_{p_{top}}^{p_s} \oint v_n ds dp = 0. \tag{11}$$

In this study, two methods will be proposed for adjusting the normal components to satisfy (11). In the first, the adjustment is proportional to the wind speed on each face:

$$v_n = v_n^* - \epsilon |\mathbf{v}^*| \tag{12}$$

where

$$\epsilon = \frac{\int_{p_{top}}^{p_s} \oint v_n^* ds dp}{\int_{p_{top}}^{p_s} \oint |\mathbf{v}^*|\, ds dp}. \tag{13}$$

The adjusted components satisfy (11). The procedure is analogous to that used by Krishnamurti et al. (1977) to obtain lateral boundary conditions for a streamfunction calculation. The corresponding divergence adjustment is proportional to mean wind speed around the polygon at each level, as seen by integrating (12) with respect to s:

$$\bar{D} - \bar{D}^* = -\frac{\epsilon \oint |\mathbf{v}^*|\, ds}{A}. \tag{14}$$

The second adjustment method simply changes v_n^* by a constant. It can easily be seen that given

$$v_n = v_n^* - C. \tag{15}$$

Equation (11) requires

$$C = \frac{\int_{p_{top}}^{p_s} \oint v_n^* ds dp}{\int_{p_{top}}^{p_s} \oint ds dp}. \tag{16}$$

The corresponding divergence adjustment at a given level is seen by integrating (15) with respect to s:

$$\bar{D} - \bar{D}^* = -\frac{C \oint ds}{A}. \tag{17}$$

Thus the constant v_n adjustment produces a divergence adjustment which is nearly constant in the vertical as well, with variation due only to the ratio of the small changes in polygon perimeter and area with height caused by convergence or divergence of the rawinsonde balloons.

A major benefit of the framework represented by (12) and (15) is that the adjustment parameter (either ϵ or C) is determined from a vertical integral of normal components, which tend to cancel, rather than determining an adjustment parameter level by level. As a result, the magnitudes of ϵ and C, and thus the fractional changes in velocity, will be shown to be small. In addition, any physical hypothesis can be inserted into (12), for instance, a rawinsonde elevation angle dependence, if an appropriate empirical form can be determined.

A measure of the effects on the integrated budgets of the form of the divergence adjustment will be determined by comparison of results using (12) and (15).

b. *Calculation procedures*

All variables are assumed to vary linearly along each edge of the polygon. This is equivalent to fitting a plane which passes through all three vertices of a triangle, or alternatively requires a linear best fit through a polygon with more than three sides (such as used by McNab and Betts 1978). In all of the calculations described below, the effect of balloon drift is incorporated by calculating the length of each edge (d) and polygon area (A) at each level according to the current positions of the rawinsondes.

The normal components are computed on each face of the polygon using (12) or (15), which represent the speed-dependent and constant adjustments, respectively. Adjusted horizontal wind vectors can be uniquely determined at each vertex from the original vector and the adjusted normal components on each edge, but such a procedure is unnecessary. Instead, the adjusted flux, divergence, and advective terms are directly computed using

$$\overline{\nabla_p \cdot q\mathbf{v}} = A^{-1} \oint q v_n ds \tag{18}$$

$$\overline{q \nabla_p \cdot \mathbf{v}} = \bar{q} \overline{\nabla_p \cdot \mathbf{v}} = \bar{q} A^{-1} \oint v_n ds \tag{19}$$

$$\overline{\mathbf{v} \cdot \nabla_p q} = \overline{\nabla_p \cdot q\mathbf{v}} - \overline{q \nabla_p \cdot \mathbf{v}} \tag{20}$$

The second step in (19) holds because $\nabla_p \cdot \mathbf{v}$ is constant across the polygon as a consequence of the assumption of linearity in the wind components. For the same reason, $\bar{q}$ is simply the average q at the vertices.

The linear variation of the normal component is given by

$$v_n = ax + b \tag{21}$$

where

$$a = \frac{v_n(x_B) - v_n(x_A)}{d} \tag{22}$$

$$b = v_n(x_A), \tag{23}$$

where subscripts A and B represent the rawinsonde positions at the vertices, and v_n values at the vertices are given by (12) or (15). Specific humidity is given by

$$q = gx + h, \tag{24}$$

where g and h are analogous to a and b above. Along a single polygon edge the flux term in (18) is thus

$$\int_x qv_n dx = \int_x (gx + h)(ax + b)dx. \tag{25}$$

The total integral around s is simply the sum of integrals along each face. A key element of the procedure is that integration is carried out analytically, which allows, within the assumption of linearity, an exact measure of eddy fluxes $\overline{q'v_n'}$ (these might be labeled "resolvable eddy fluxes"). It is shown in Appendix A that substitution of finite difference procedures for (25) can produce errors approaching 50 percent for commonly observed gradients of the quantities in question. Although unresolvable eddy fluxes exist as well, due to the departure of variables in nature from the assumed linear variation, the evidence suggests that consistent use of analytical integrations along polygon edges provides a significant improvement over finite difference methods. Because all variables are assumed to vary linearly along each edge, analytical and finite difference calculations give the same result for integration of a single variable; the difference noted in Appendix A arises only in the nonlinear terms in (18) and (20) (except in the near-surface layers; see appendix B).

Pressure integrals are carried out using the midpoint rule. Special attention must be paid to vertical integration over the layers below the lowest common pressure level of the stations in the polygon, because the lower boundary is not a constant-pressure surface. Appendix B describes the integration method for the lowest layers.

c. Data sources

Three-hourly rawinsonde data from the SESAME experiment were used from two regional scale days (19–20 and 25–26 April 1979) and three storm-scale days (9–10 and 20–21 May and 7–8 June 1979), which are composed of a high-resolution inner network (mean station separation of ~90 km) and, except for 20–21 May, a regional scale network. As noted by Fankhauser (1974), manual editing of each individual sounding contributed significantly to the quality of the final dataset. No obvious errors existed that could not be removed by objective methods, but not all errors could be anticipated without manual editing of the dataset. The errors discovered were few, but included relative humidity exceeding 100 percent, an abrupt shift of wind components of >50 m s^{-1} over 25 mb, and a sudden zeroing of the balloon drift or potential temperature at a single level. If such errors could easily be corrected, for instance, by interpolation from immediately adjacent vertical levels, the sounding was retained; otherwise the sounding was removed from the dataset.

The data were linearly interpolated to produce 25 mb resolution in the vertical, up to a p_{top} of 125 mb. Surface values were retained as well. The resultant soundings were arranged into triangles of varying scales, each of which was then treated separately, as would be the case for an isolated polygon of stations. A large set of unique (but overlapping) triangles was formed which satisfied the following criteria:

(i) Release time of the balloons for the three stations at the vertices within 20 minutes of a common time;
(ii) No angle of the triangle less than 30°, in order to avoid strongly oblique triangles; and
(iii) Data available up to 125 mb at all three stations.

Approximately 30,000 triangles ranging in scale from 1.4×10^9 to 1×10^{12} m^2 (equivalent in area to equilateral triangles with sides from 53 to 1414 km) were produced by the above procedure; these form the basis for most of the calculations. Although the entire dataset comes from a single geographical area, it encompasses a wide variety of dynamical and thermodynamical environments, ranging from no rainfall over the network to intense rainfall, and from stable nighttime to unstable daytime boundary layers. The results should provide a reasonable measure of the sensitivity of budget calculations in a middle latitude convective environment.

4. Results

a. Adjustment parameters

Table 1 shows the cumulative percentage of triangles with $|\epsilon|$ less than a given value. More than 95 percent of triangles had $|\epsilon| < 0.1$, with the median value 0.03, insuring that the percentage change in the wind vector for the speed-dependent adjustment was almost always small. Triangles or polygons of data in diagnostic studies are often rejected when their integrated divergence exceeds a certain value (e.g., Frank 1979). Because ϵ can be small when integrated divergence is large [see Eq. (13)], it may provide a better rejection parameter for individual polygons than integrated divergence itself.

Table 2 gives an analogous distribution of values for the constant normal component adjustment [Eq. (16)]. Fewer than 2% of these values exceeded 2 m s^{-1}, with a median value of less than 0.5 m s^{-1}. As with the speed-dependent adjustment, the magnitude of the vector change of the wind at a given point remained small.

Figure 1 shows vertical profiles of wind speed for the five SESAME periods used in this study, and thus,

TABLE 1. Number of triangles in each range of ϵ values, and cumulative percentage of triangles with $|\epsilon|$ less than the value shown.

$\lvert\epsilon\rvert$ Range	Number of triangles	Cumulative percentage
0–.01	5934	19.2
.01–.02	5373	36.7
.02–.03	4440	51.1
.03–.04	3728	63.2
.04–.05	2957	72.7
.05–.06	2347	80.4
.06–.07	1711	85.9
.07–.08	1294	90.1
.08–.09	1007	93.4
.09–.10	656	95.5
.10–.11	447	96.9
.11–.12	313	98.0
.12–.13	204	98.6
.13–.14	151	99.1
All others	306	100.0

TABLE 2. Distribution of values of the constant normal component adjustments [m s^{-1}, from Eq. (16)] required to achieve zero integrated divergence.

v_n Adjustment (m s^{-1})	Number of triangles	Cumulative percentage
0–0.1	3679	11.9
0.1–0.2	3632	23.7
0.2–0.3	3214	34.1
0.3–0.4	2979	43.8
0.4–0.5	2660	52.4
0.5–0.6	2272	59.8
0.6–0.7	2066	66.5
0.7–0.8	1704	72.0
0.8–0.9	1443	76.7
0.9–1.0	1328	81.0
1.0–1.1	1084	84.5
1.1–1.2	935	87.6
1.2–1.3	817	90.2
1.3–1.4	612	92.2
1.4–1.5	515	93.8
1.5–1.6	449	95.3
1.6–1.7	305	96.3
1.7–1.8	241	97.1
1.8–1.9	175	97.6
1.9–2.0	158	98.2

by virtue of (14), also shows the mean divergence adjustment profiles for the speed-dependent adjustment. It is apparent from Fig. 1 that the speed-dependent and constant [Eq. (17)] adjustments differ significantly during all time periods studied. As a result, the median difference in precipitation rate estimated from the two should provide a reasonable estimate of the error caused by the lack of knowledge of the true divergence adjustment profile.

b. *Precipitation errors*

The errors in calculated precipitation arising from neglect of the advecting velocity adjustment [Eqs. (8) and (9)] were found to be negligible for both heat and moisture budgets, with median values less than 0.02 cm day^{-1}, and fewer than 1% exceeding 0.5 cm day^{-1}. This result reflects the fact that although horizontal advection changes at a point when velocity is adjusted, the area-averaged advection changes by much less, because only normal components of the wind are adjusted around the edge, and these adjustments tend to cancel. It is easily seen that for an equilateral triangle and a constant normal component adjustment along the edges, neither $\bar{u}$ nor $\bar{v}$ changes. Because the horizontal gradients of q and θ are constant over the triangle by the assumption of linearity, the change in mean advection due to the divergence adjustment can be written

$$-\overline{\Delta\mathbf{v}\cdot\nabla\theta} = -\overline{\Delta\mathbf{v}}\cdot\overline{\nabla\theta}$$

with a comparable expression for q, where $\overline{\Delta\mathbf{v}}$ is the change in the mean wind vector over the polygon. As noted earlier, for an equilateral triangle both components of $\overline{\Delta\mathbf{v}}$ vanish, and thus advection is unchanged by adjustment of the divergence. For an oblique triangle, the normal component adjustments no longer exactly cancel, and a small change in mean velocity occurs which slightly alters the horizontal advection. As an example, if the constant normal component adjustment is 0.4 m s^{-1} (near its median value), the change of the mean advecting velocity ($\overline{\Delta\mathbf{v}}$) amounts to only 0.2 m s^{-1} for a 30°–60°–90° triangle. The effect of this small change in advecting velocity is further reduced by cancellations of $-\overline{\Delta\mathbf{v}}\cdot\overline{\nabla\theta}$ in the vertical integration. As a result, the vertically integrated mean advection over a polygon changes little when diver-

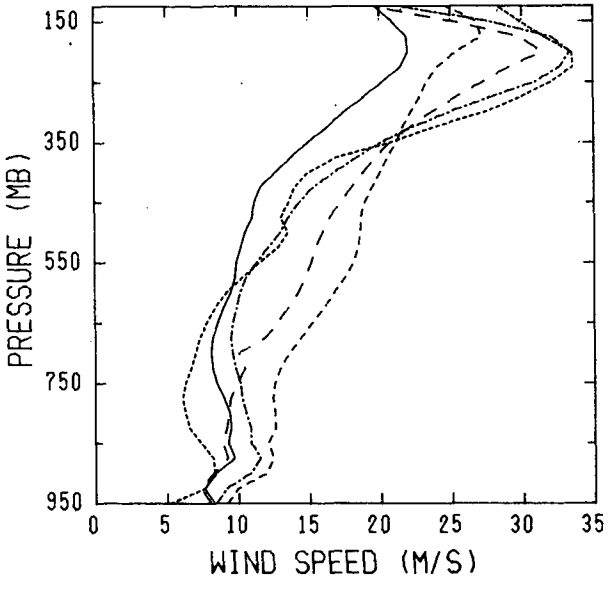

FIG. 1. Mean vertical profiles of wind speed for the five SESAME periods studied. Solid: 19–20 April, large dash: 25–26 April, medium dash: 9–10 May, small dash: 20–21 May, dash-dot: 7–8 June (all are 1979).

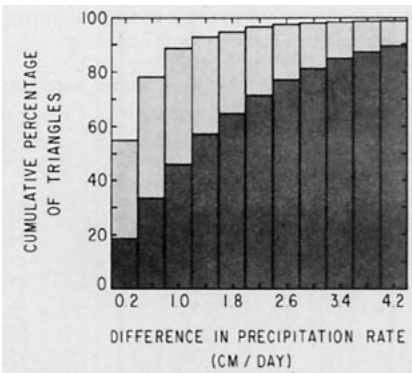

FIG. 2. Distribution of differences in calculated precipitation (cm day^{-1}) produced by two differing divergence adjustment profiles, for the heat budget (dark shading) and the moisture budget (light shading). The bars represent the cumulative percentage of triangles with differences less than the values given on the horizontal axis.

gence is adjusted to satisfy mass balance. Precipitation estimates are little influenced by neglect of the advecting velocity adjustment, even when the unadjusted integrated divergence is large.

Figure 2 shows the distribution of differences in calculated precipitation using the two divergence adjustment profiles represented by (12) and (15). Table 3 gives the median difference and frequency of extreme errors in precipitation estimate, for the entire dataset and for triangles with areas exceeding 2×10^{11} m^2 (equivalent to equilateral triangles with sides greater than 632 km), which make up about half of the total. The results show that:

(i) Errors caused by the choice of the divergence adjustment profile greatly exceed those produced by neglect of the advecting velocity adjustment;

(ii) Heat budget errors exceed moisture budget errors by a factor of four;

(iii) Errors exceeding 5 cm day^{-1}, which are unacceptably large except in regions of strong forcing, occur much more frequently in the heat budget;

TABLE 3. Median differences in precipitation estimate [cm day^{-1}, from Eqs. (8) and (9)] and percentage of triangles with differences exceeding 5 cm day^{-1}, between budget calculations utilizing speed-dependent and constant divergence adjustment profiles. The values provide an approximate measure of the error which arises because the true divergence adjustment profile is unknown. Under "large areas" are median differences in a subset of triangles with areas in excess of 2×10^{11} m^2, which make up about 50% of the dataset.

	Median error		Percentage of triangles with errors exceeding 5 cm day^{-1}	
	Entire	Large areas	Entire	Large areas
q budget	0.35	0.31	1.3	0.0
θ budget	1.34	1.21	8.1	2.2

(iv) The areal dependence of the errors associated with the choice of the divergence adjustment profile was weak, with only a 10% reduction in error for the largest half of the triangles in the dataset.

The reasons for the larger errors caused by the choice of divergence adjustment profile in the heat budget can be seen by taking the ratio of such errors between the moisture and heat budgets using (8) and (9), but for a single level:

$$\frac{\text{moisture budget error}}{\text{heat budget error}} \approx \frac{L \int_{p_{top}}^{p_s} q \Delta v_n \oint ds dp}{C_p \int_{p_{top}}^{p_s} T \Delta v_n \oint ds dp} \tag{26}$$

where the divergence theorem has been used, T/θ has been moved inside the ∇_p operator and the difference in normal components Δv_n between the two methods has been assumed to be constant around the triangle. The ratio of the pressure integrands in (26) rarely exceeds 0.1, and reaches 0.01 in the upper troposphere. Thus the error in precipitation estimate, which depends on the vertical integral of each variable weighted by Δv_n, would be expected to be an order of magnitude larger in the heat budget than the moisture budget, simply because each term in the vertical sum is that much larger.

Table 3 shows that the heat budget terms are larger, but only by a factor of four. This reduction of the expected error can be seen heuristically by the following reasoning. The quantity Δv_n must change sign with height, because its vertical integral must be zero in order that both adjustment methods satisfy zero integrated divergence [Eq. (11)]. Examination of Fig. 1 shows that the constant and linearly increasing divergence adjustments should be accompanied by Δv_n of one sign below and the opposite sign above. In the heat budget, temperature varies by less than 50% from top to bottom of the troposphere, and thus partial cancellation occurs between lower and upper levels. In the moisture budget, however, upper level contributions are negligible, cancellation does not occur, and thus integrated errors exceed those associated with a more uniform vertical profile. The result of the two effects is that heat budget errors are larger, but by less than what simple order of magnitude arguments would give.

5. Discussion and conclusions

Kuo and Anthes (1984) determined typical differences in vertically integrated heat and moisture sources and sinks between numerical model-generated observations and diagnostic budget estimates for a regional scale day in SESAME, averaged over 550 × 550 km and six hours. These total budget errors, which include the effects of inadequate data resolution, measurement and analysis errors, and neglect of liquid water storage, amounted to 5 K day^{-1} in the heat budget and 2 gm

kg^{-1} day^{-1} ($\sim$1.7 cm day^{-1}) in the moisture budget. These errors should provide a lower limit for total budget errors in individual triangles at a given time, because (i) Kuo and Anthes filtered out all waves of period less than six hours, which may otherwise have contributed significantly to budget errors in the highly convective situation; and (ii) the Cressman objective analysis scheme used by Kuo and Anthes produced spatial smoothing of all fields, while the triangle approach uses data as measured, except for limited vertical interpolation. As a result, it will be assumed that the errors arising from calculation procedures in this study are negligible if they are less than 20 percent of the total budget errors of Kuo and Anthes (1984).

By any reasoning, errors due to neglect of the horizontal advecting velocity adjustment will be negligible when averages over a polygon of data points are considered. By implication, such errors would also be negligible for gridded calculations when averaged over more than a single grid point.

The choice of divergence adjustment profile produced a median difference in the moisture budget estimate of precipitation which is marginally negligible by the above reasoning. In the heat budget, however, errors were the same order as overall budget errors of Kuo and Anthes. The larger errors in the heat versus moisture budgets were attributed to roundoff error, because heat budget terms are an order of magnitude larger than moisture budget terms. This does not necessarily mean that actual computed precipitation values will be less accurate in the heat budget, only that this one source of error is larger.

The true divergence error profile in nature is unknown. As a result, the differences in precipitation arising from the choice of the divergence adjustment profile, which reached 1.34 and 0.35 cm day^{-1} in the heat and moisture budgets, respectively, appear to represent minimum median errors in diagnosed precipitation in middle latitude convection.

This study utilized analytical integrations along polygon edges, thus providing an exact measure of eddy fluxes, within the assumption of linearity. The substitution of finite difference methods in flux and advective terms was shown to introduce large errors when the analyzed quantities had large horizontal gradients. For studies involving isolated polygons of data, for which analytical procedures can easily be adopted, analytical integration provides significant benefits over finite differencing.

The divergence calculations in this study incorporated the effects of balloon drift via the changing size of triangles with height. As a result, the associated volumes have tilted, not straight, sides in the vertical. The constraint of near-zero integrated divergence does not necessarily hold for tilted volumes, particularly for small triangles in high speed flow. Table 3 shows, however, that large triangles had errors similar to those diagnosed for the entire dataset, implying that the overall results were unaffected by the tilting of small volumes.

Although calculations were made only for triangles, all the equations apply directly to n-sided polygons as well, provided a linear best-fit is used (McNab and Betts 1978) and observed values are replaced with their best fit values at the vertices. The approach cannot, however, be used on a grid in the form given. Adjacent grid boxes would have differing v_n adjustments on their common side, because the adjustment depends on the wind field within each grid box. In principle, an iterative procedure could be developed using the current approach, along the lines of that by Endlich (1967), but great care would be required to maintain finite difference consistency with other calculations, and the benefits over other grid methods would be questionable. Nevertheless, the results of this study remain valid for gridded calculations. As an example, Fuelberg et al. (1986) estimated precipitation from an integrated moisture budget in SESAME on a high resolution grid while neglecting the adjustment of horizontal advecting velocity required by the adjusted divergence. The results of this study suggest that no meaningful error resulted from that simplification.

Because divergence error might be expected to increase with increasing wind speed, the speed-dependent profile of divergence adjustment is physically more realistic than the (nearly) constant profile, and also more consistent with the typical increase of rawinsonde measurement error with height (Barnes, 1981). Nevertheless, for reasons put forth by Pedder (1981), the speed-dependent profile may not be more accurate in practice. A logical extension of this study would compare observed precipitation to that computed using Eq. (2) (or its heat budget equivalent), to determine what form of divergence adjustment profile produced the most accurate estimate of precipitation. Observed precipitation itself contains significant errors, however, and (2) requires knowledge of local time derivatives, whose accuracy is questionable when finite differences over six hours or more must be used. Because median differences in precipitation rate arising from the form of the divergence adjustment amounted to less than 1 mm h^{-1}, determination of an optimum divergence error profile for diagnostic studies may not be possible using currently available data.

Acknowledgments. We thank Dr. William Frank of the Department of Meteorology at Pennsylvania State University for his critical review of the manuscript. We appreciate the efforts of an anonymous reviewer, whose comments contributed to development of a less complex form for the speed-dependent adjustment than in the original manuscript. The SESAME data for this study were provided by Dr. J. J. Stephens of the Department of Meteorology at Florida State University. This research is supported by National Science Foundation Grant ATM-8603241.

APPENDIX A

Analytical Versus Finite Difference Integration

The flux of specific humidity along a single polygon edge is written

$$F = \int_x qv_n dx \tag{A1}$$

where

$$v_n = ax + b, \tag{A2}$$

$$q = gx + h, \tag{A3}$$

a, b, g and h are constants, and x is the distance along the edge. Without loss of generality, the edge will be assumed to be of unit length, and a bar operator is defined by

$$(\bar{\ }) = \int_0^1 (\ )dx. \tag{A4}$$

Using (A2)–(A4), the analytical expression for (A1) becomes

$$\overline{qv_n} = \frac{aq}{3} + \frac{1}{2}(ah + bg) + bh. \tag{A5}$$

Two finite difference approximations will be compared to the exact solution (A5). The first estimates $\overline{qv_n}$ by its average at the end points, i.e.,

$$(\overline{qv_n})_{\mathrm{I}} = \frac{1}{2}\{(qv_n)_0 + (qv_n)_1\} \tag{A6}$$

while the second uses

$$(\overline{qv_n})_{\mathrm{II}} = \bar{q}\,\overline{v_n} \tag{A7}$$

and thus explicitly omits the eddy flux $\overline{q'v_n'}$. It is easily seen using (A2) and (A3) that (A6) can be written

$$(\overline{qv_n})_{\mathrm{I}} = \frac{1}{2}(ag + ah + bg) + bh \tag{A8}$$

and the error introduced by the finite difference form (A6) is

$$\overline{qv_n} - (\overline{qv_n})_{\mathrm{I}} = -\frac{1}{6}ag. \tag{A9}$$

The error is proportional to the product of the gradients of the two variables making up the flux term. The finite difference estimate is exact only when one or both variables are constant along the edge. The analogous finite difference error in (A7)is

$$\overline{qv_n} - (\overline{qv_n})_{\mathrm{II}} = -\frac{1}{12}ag. \tag{A10}$$

Both of these errors can become large under fairly ordinary circumstances. If v_n varies from -10 to $+6$ m s^{-1}, and q varies from 10 to 6 g kg^{-1}, the errors from (A9) and (A10) amount to 50 percent and 25 percent of the exact solution, respectively.

APPENDIX B

Calculation Procedures Required by Varying Surface Pressure

Special procedures are required at the earth's surface, which is not a constant-pressure surface. Figure B1 gives a schematic example of varying surface pressure across a triangle. The procedure below is required because a given normal component in the low layers transports varying amounts of mass depending upon the pressure depth of the layer between the surface and the first common pressure level (p_c) of the three stations making up the triangle. The layer beneath the first common pressure level will be referred to in this appendix as the "surface layer," but does not relate to the constant flux layer of the same name in boundary layer theory.

As noted in the text and in Appendix A, analytical integration, although used on all terms, differs from finite difference integration only for the nonlinear flux and advective terms. In the surface layer, however, the variable pressure difference between p_s and p_c will also be incorporated analytically, and thus all vertical integrals become nonlinear in this layer. For example, the unadjusted, area-averaged integrated divergence $\bar{D}^*$ is divided into two parts:

$$\int_{p_{\mathrm{top}}}^{p_s} \bar{D}^* dp = \int_{p_c}^{p_s} \bar{D}^* dp + \int_{p_{\mathrm{top}}}^{p_c} \bar{D}^* dp. \tag{B1}$$

Using Eq. (10) in the paper, the surface layer integral is written

$$\int_{p_c}^{p_s} \bar{D}^* dp = A^{-1} \oint \int_{p_c}^{p_s} v_n^* dpds \tag{B2}$$

where v_n^* is the unadjusted normal wind component, and the order of integration has been reversed under the assumption that the change in triangle perimeter

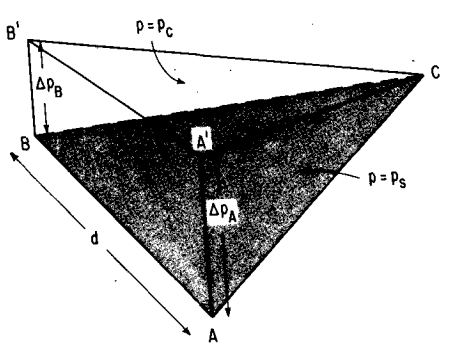

FIG. B1. Schematic diagram of a triangle of stations (at A, B and C) with varying surface pressures. The surface ABC (shaded) represents $p = p_s$ and $A'B'C$ represents the first common pressure level p_c. The vertical tilt is exaggerated; in practice, $A'C \approx AC$, $A'B' \approx AB$.

due to balloon drift can be neglected near the ground. Because both v_n^* and dp vary with s, the integral in (B2) is written

$$\frac{1}{A}\oint\int_{p_c}^{p_s} v_n^* dpds = \frac{1}{A}\sum_{i=1}^{N}\int_{x_A}^{x_B} (\tilde{v}_n^*)_i \Delta p_i dx_i \quad \text{(B3)}$$

where i is the index for each polygon face, N the number of faces, and $\tilde{v}_n^*$ the mean normal component in the layer p_s to p_c. Along each face it is assumed that $\tilde{v}_n^*$ and Δp vary linearly, and (B3) is integrated analytically, as described in Eq. (25) of the paper.

Once unadjusted integrated divergence is determined, the normal components $\tilde{v}_n^*$ are adjusted using (12) or (15), and integrated divergence is recalculated to insure that it vanishes, i.e., to check the internal consistency of the procedure. The surface layer flux, divergence, and advective terms are carried out as in (18)–(20), but with the variation of surface pressure included. For example, the surface layer moisture flux term along a polygon edge is

$$\int_x\int_{p_c}^{p_s} qv_n dpdx = \int_x q\tilde{v}_n \Delta p dx$$

$$= \int_x (gx + h)(ax + b)(rx + s)dx \quad \text{(B4)}$$

where (g, h), (a, b), and (r, s) represent the linear variation of q, $\tilde{v}_n$ and Δp, respectively. The resulting expression is easily integrable.

REFERENCES

Barnes, S. L., Ed., *SESAME 1979 Data Users Guide.* NOAA/ERL, Boulder, CO, 236 pp.

Endlich, R. M., 1967: An iterative method for altering the kinematic properties of wind fields. *J. Appl. Meteor.*, **6**, 837–844.

Fankhauser, J. C., 1974: The derivation of consistent fields of wind and geopotential height from mesoscale rawinsonde data. *J. Appl. Meteor.*, **13**, 637–646.

Frank, W. M., 1979: Individual time period analyses over the GATE ship array. *Mon. Wea. Rev.*, **107**, 1600–1616.

Fuelberg, H. E., Y. Lin and H. Chang, 1986: A moisture analysis of the meso-β scale thunderstorm environment during AVE-SESAME V (20–21 May 1979). *Mon. Wea. Rev.*, **114**, 534–545.

Kuo, Y. H., and R. A. Anthes, 1984: Accuracy of diagnostic heat and moisture budgets using SESAME-79 field data as revealed by observing system simulation experiments. *Mon. Wea. Rev.*, **112**, 1465–1481.

Krishnamurti, T. N., J. Molinari and H. L. Pan, 1977: Numerical simulation of the Somali jet. *J. Atmos. Sci.*, **33**, 2350–2362.

——, H. L. Pan, C. B. Chang, J. Ploshay, D. Walker and A. W. Oodally, 1979: Numerical weather prediction for GATE. *Quart. J. Roy. Meteor. Soc.*, **105**, 979–1010.

McNab, A. L., and A. K. Betts, 1978: A mesoscale budget study of cumulus convection. *Mon. Wea. Rev.*, **106**, 1317–1331.

Nitta, T., 1977: Response of cumulus updraft and downdraft to GATE A/B scale motion systems. *J. Atmos. Sci.*, **34**, 1163–1186.

O'Brien, J. J., 1970: Alternative solutions to the classical vertical velocity problem. *J. Appl. Meteor.*, **9**, 197–203.

Pedder, M. A., 1981: On the errors of kinematic vertical motion estimation using divergence bias adjustment procedures. *Mon. Wea. Rev.*, **109**, 1813–1816.

Ray, P. S., C. L. Ziegler, W. Bumgarner and R. J. Serafin, 1980: Single- and multiple-Doppler radar observations of tornadic storms. *Mon. Wea. Rev.*, **108**, 1607–1625.

Smith, P. J., 1971: An analysis of kinematic vertical motions. *Mon. Wea. Rev.*, **99**, 715–724.

Stephens, J. J., 1968: Variational resolution of wind components. *Mon. Wea. Rev.*, **96**, 229–231.